Proc. Natl. Acad. Sci. USA
Vol. 96, pp. 10637–10642, September 1999
Biochemistry

Detoxification of environmental mutagens and carcinogens: Structure, mechanism, and evolution of liver epoxide hydrolase

(protein crystallography/α/β hydrolase/domain swapping)

MARIA A. ARGIRIADI*, CHRISTOPHE MORISSEAU†, BRUCE D. HAMMOCK†, AND DAVID W. CHRISTIANSON*‡

*Roy and Diana Vagelos Laboratories, Department of Chemistry, University of Pennsylvania, Philadelphia, PA 19104-6323; and †Department of Entomology, University of California, Davis, CA 95616

Edited by William N. Lipscomb, Harvard University, Cambridge, MA, and approved July 19, 1999 (received for review June 4, 1999)

ABSTRACT **The crystal structure of recombinant murine liver cytosolic epoxide hydrolase (EC 3.3.2.3) has been determined at 2.8-Å resolution. The binding of a nanomolar affinity inhibitor confirms the active site location in the C-terminal domain; this domain is similar to that of haloalkane dehalogenase and shares the α/β hydrolase fold. A structure-based mechanism is proposed that illuminates the unique chemical strategy for the activation of endogenous and man-made epoxide substrates for hydrolysis and detoxification. Surprisingly, a vestigial active site is found in the N-terminal domain similar to that of another enzyme of halocarbon metabolism, haloacid dehalogenase. Although the vestigial active site does not participate in epoxide hydrolysis, the vestigial domain plays a critical structural role by stabilizing the dimer in a distinctive domain-swapped architecture. Given the genetic and structural relationships among these enzymes of xenobiotic metabolism, a structure-based evolutionary sequence is postulated.**

During the course of mammalian evolution, myriad catabolic pathways have evolved to defend against harmful environmental chemicals and their metabolites. For example, aromatic hydrocarbons such as styrene, stilbene, or benzo[*a*]pyrene can be oxidized *in vivo* to form mutagenic epoxides that readily alkylate nucleic acids. Olefinic terpenoid natural products can be similarly activated and oxidized to generate terpenoid epoxides with various reactivities and potencies (1). The first line of chemical defense against xenobiotic-derived epoxides is the liver enzyme epoxide hydrolase (EC 3.3.2.3) (1–3), which exists as microsomal and soluble enzymes designated mEH and sEH, respectively; sEH is found in both the cytosol and the peroxisomal matrix of liver cells (4–8). Both mEH and sEH hydrolyze epoxides to form vicinal 1,2-diols, which are typically less reactive, less mutagenic, and more rapidly excreted due to increased solubility (1, 9). Accordingly, sEH activity is found to decrease the mutagenicity of epoxides in the Ames *Salmonella* assay (10), and it decreases the induction of sister chromatid exchange by *trans*-β-ethylstyrene (11).

The catalytic mechanism of sEH proceeds through a covalent alkylenzyme ester intermediate with an active site aspartate nucleophile. Strikingly, hydrolysis of this intermediate requires that an oxygen atom of the enzyme is incorporated into the vicinal diol product with each turnover (12–14). Enzymological studies of the related mEH isozyme (21% sequence identity) indicate an identical mechanism proceeding through an alkylenzyme ester intermediate (15–17). Interestingly, GJ10 haloalkane dehalogenase (18–21) and haloacid dehalogenase (22–24) from *Xanthobacter autotrophicus* each hydrolyze carbon–halogen bonds through mechanisms similarly involving an aspartate nucleophile and an alkylenzyme ester intermediate. These are the first and last enzymes, respectively, in the catabolism of 1,2-dihalogenated alkanes such as 1,2-dichloroethane and 1,2-dibromoethane. Like the parent styrene oxide of *trans*-substituted sEH substrates, these halogenated alkanes have been classified by the U.S. Environmental Protection Agency as hazardous air pollutants under section 112 of the Clean Air Act Amendments of 1990 (42 U.S.C. §7412) and are probable human carcinogens (25).

The bacterial dehalogenases are genetically and topologically unrelated to each other, but each is seen to bear an individual and distant evolutionary relationship with sEH suggestive of an early gene fusion event (5). Haloalkane dehalogenase is a member of the α/β hydrolase family (19–21, 26) and shares 20% sequence identity with the C-terminal domain of sEH (5). Haloacid dehalogenase adopts an unrelated α/β fold (27, 28) and shares 20% sequence identity with the N-terminal domain of sEH (5, 29). Despite inconclusively weak amino acid sequence identities, sequence gazing indicates conservation of the key catalytic nucleophile of each dehalogenase in both domains of sEH: Asp-8 of haloacid dehalogenase aligns with Asp-9 in sEH, and Asp-124 of haloalkane dehalogenase aligns with Asp-333 in sEH (5, 18, 29).

It is curious that the sEH monomer contains two possible active sites—which one is involved in the catalytic hydrolysis of epoxide substrates? Moreover, how closely are the two possible active sites of sEH related to the individual active sites of haloalkane dehalogenase and haloacid dehalogenase? Finally, what is the chemical strategy to activate the epoxide ring for catalytically efficient nucleophilic attack? To address these questions, we now report the x-ray crystal structure of recombinant murine sEH (30, 31) determined by multiple isomorphous replacement and refined at 2.8-Å resolution (Tables 1 and 2). Additionally, the complex of sEH with the dialkylurea inhibitor *N*-cyclohexyl-*N*′-(3-phenyl)propylurea [CPU; K_i = 3.1 nM (32)] has been determined at 2.8-Å resolution.

MATERIALS AND METHODS

Recombinant murine sEH was crystallized by equilibrating 5.0 μl of protein solution [16 mg/ml sEH, 3 mM DTT, 100 mM sodium phosphate (pH 7.4)] with 4.5 μl of precipitant buffer [1.6 M ammonium sulfate, 100 mM Mes (pH 6.0)] and 0.5 μl of ethanol [final concentration = 1.4% (vol/vol)] in a hanging drop suspended over a 1-ml reservoir of precipitant buffer at room temperature. Plate-like crystals with approximate di-

The publication costs of this article were defrayed in part by page charge payment. This article must therefore be hereby marked "*advertisement*" in accordance with 18 U.S.C. §1734 solely to indicate this fact.

PNAS is available online at www.pnas.org.

This paper was submitted directly (Track II) to the *Proceedings* office.
Abbreviations: sEH, soluble epoxide hydrolase; CPU, *N*-cyclohexyl-*N*′-(3-phenyl)propylurea.
Data deposition: The atomic coordinates have been deposited in the Protein Data Bank, www.rcsb.org (PDB ID codes 1CQZ for sEH and 1CR6 for sEH–CPU complex).
‡To whom reprint requests should be addressed. E-mail: chris@xtal.chem.upenn.edu.

Table 1. Data collection

Data set	Resolution, Å	Reflections measured/unique	Completeness, %, overall/outer shell	R_{merge}* overall/outer shell	R_{iso}†	No. of sites‡	Phasing power§	Overall figure of merit (3.0 Å)
Native sEH	2.8	304,577/32,278	99.0/96.7	0.070/0.357	—	—	—	
sEH–CPU complex	2.8	73,807/24,877	80.1/42.8	0.096/0.345	—	—	—	
K_2UOF_6	3.0	69,813/24,494	89.9/84.9	0.060/0.089	0.195	2	1.05	
Samarium(III) acetate	3.5	43,302/15,970	91.4/89.6	0.104/0.310	0.252	2	0.85	
Trimethyl-lead acetate, 1-week soak	3.1	96,185/20,906	83.3/84.1	0.104/0.440	0.198	2	0.84	
Trimethyl-lead acetate, 1-day soak	2.9	77,792/24,930	80.7/76.0	0.063/0.290	0.109	2	0.80	
Mercuric acetate	2.9	84,495/28,967	96.8/91.3	0.078/0.353	0.226	2	0.54	
$K_2Pt(CNS)_6$	3.4	52,353/17,253	90.5/89.1	0.112/0.322	0.240	4	0.38	
								0.468

*$R_{merge} = \Sigma|I_i - \langle I_i\rangle|/\Sigma|\langle I_i\rangle|$, where I_i is the intensity measurement for reflection i, and $\langle I_i\rangle$ is the mean intensity calculated for reflection i from replicate data.
†$R_{iso} = \Sigma||F_{PH}| - |F_P||$, where F_{PH} and F_P are the derivative and native structure factors, respectively.
‡Per monomer.
§Phasing power = $\langle F_H\rangle/E$ where $\langle F_H\rangle$ is the root-mean-square heavy-atom structure factor and E is the residual lack of closure error.

mensions 0.5 mm × 0.3 mm × 0.1 mm appeared within 1 week and diffracted x-rays to 2.8-Å resolution with synchrotron radiation. They belong to space group $P2_12_12$ with unit cell parameters a = 151.9 Å, b = 143.0 Å, c = 60.0 Å (one dimer in the asymmetric unit). Crystals of the sEH–CPU complex were prepared by soaking in a precipitant buffer solution containing 5 mM CPU for 4 days.

Diffraction data were collected from flash-cooled crystals by using Area Detector Systems Corporation charge-couple device area detectors at the Cornell High Energy Synchrotron Source (beamline A-1) and the Brookhaven National Light Source (beamline X12B). Data reduction was achieved with DENZO and SCALEPACK (33). For phasing by multiple isomorphous replacement (MIR), initial heavy atom positions were determined in difference Patterson maps and refined with the program MLPHARE in the CCP4 suite (Table 1) (34). The model was fit into an electron density map calculated with solvent-flattened noncrystallographic symmetry (NCS)-averaged MIR phases at 3.0-Å resolution by using SOLOMON (35). Subsequent refinement and rebuilding of the native model were achieved with X-PLOR (36) and O (37), respectively. Individual B factors were refined and a bulk solvent correction was applied. In the final stages of refinement, the quality of the model was improved by gradually releasing the NCS constraints (w = 1000 kcal/mol·Å^2) into weighted restraints (w = 10 kcal/mol·Å^2) as judged by R_{free}. In the final model of the sEH dimer, the N-terminal Met-1–Leu-3 and the C-terminal Val-545–Ile-554 segments are disordered in both monomers. Additionally, monomer A contains two disordered loops: Ala-20–Glu-47 and Val-64–Ser-89. Per monomer, only 3 of 541 modeled residues adopt disallowed conformations. Refinement statistics are recorded in Table 2. The atomic coordinates of native sEH and the sEH–CPU complex have been deposited in the Research Collaboratory for Structural Bioinformatics (RCSB) with accession codes 1CQZ and 1CR6, respectively.

RESULTS AND DISCUSSION

Structure and Catalytic Mechanism. The sEH dimer has approximate dimensions 85 Å × 75 Å × 60 Å and is stabilized by a domain-swapped architecture (Fig. 1). Each 62.5-kDa monomer is composed of two principal domains: the vestigial domain (N-terminal, Arg-4–Gly-218), which does not participate in epoxide hydrolysis; and the catalytic domain (C-terminal, Val-235–Ala-544). The catalytic domain exhibits a fold similar to that of the epoxide hydrolase from *Agrobacterium radiobacter* AD1, which lacks the N-terminal domain of the larger mammalian hydrolase; unfortunately, the structure of the bacterial hydrolase was determined in an inactive conformation (38). The vestigial and catalytic domains adopt unrelated α/β folds and are connected by a 16-residue, proline-rich linker (Thr-219–Asp-234).

Inhibitor binding in the sEH–CPU complex indicates that the active site for epoxide hydrolysis resides in the C-terminal domain, which we accordingly designate the catalytic domain (Fig. 1). The catalytic domain of sEH adopts the α/β hydrolase fold (26) similar in topology to that of haloalkane dehalogenase (19, 20). The active site of sEH is located at the base of a 25-Å-deep, L-shaped cavity; this cavity contains a hydrophobic pocket at the base of the "L" (Fig. 2). No major structural changes occur in the active site upon inhibitor binding, nor are there any significant tertiary or quaternary structural changes elsewhere in the sEH dimer. An unexpected *trans,cis*-dialkyl conformation is sterically required to fit the 15-Å-long inhibitor into the L-shaped active site cavity. Catalytic nucleophile Asp-333 is located near the bend of the "L". The only hydrogen bond made in the enzyme–inhibitor complex occurs between the phenolic hydroxyl group of Tyr-465 and the *cis*-isomerized urea nitrogen. The inhibitor cyclohexyl group binds deep in the hydrophobic pocket, and the phenylpropyl moiety of CPU extends toward the mouth of the active-site cavity; both take part in numerous van der Waals interactions with aliphatic and aromatic active-site residues. These binding interactions explain the structural preference for large inhibitor substituents that are complementary in size and shape to the hydrophobic pocket (39–42). Moreover, the high-affinity binding interactions of CPU explain why environmental exposure to commonly used alkylurea pesticides and herbicides can inhibit human liver sEH, which could pose

Table 2. Refinement statistics

Protein	Atoms	Solvent molecules	Resolution, Å	No. reflections work/free	R/R_{free}*	Root-mean-square deviations			
						Bonds, Å	Angles, °	Dihedrals, °	Impropers, °
sEH	8,178	40	2.8	30,555/1,598	0.214/0.309	0.014	1.9	27.7	1.0
sEH-CPU complex	8,216	21	2.8	22,648/1,153	0.201/0.312	0.013	1.8	27.2	0.9

*$R = \Sigma||F_o| - |F_c||/\Sigma|F_o|$, where R and R_{free} are calculated by using the working and test reflection sets, respectively.

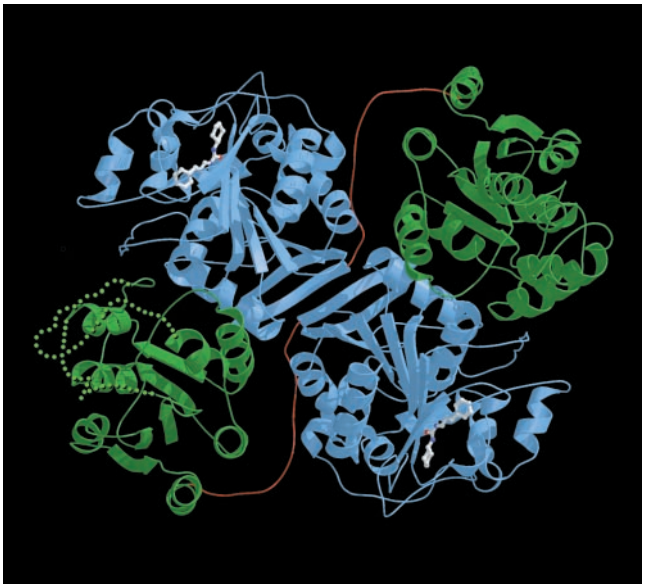

FIG. 1. Ribbon plot of the epoxide hydrolase dimer, color-coded as follows: C-terminal catalytic domain, blue; N-terminal vestigial domain, green; and linker, red. Dotted green lines indicate the disordered Ala-20–Glu-47 and Val-64–Ser-89 segments in monomer A. The location of the active site is indicated by the bound inhibitor CPU. This figure was prepared with BOBSCRIPT and RASTER3D (47–49).

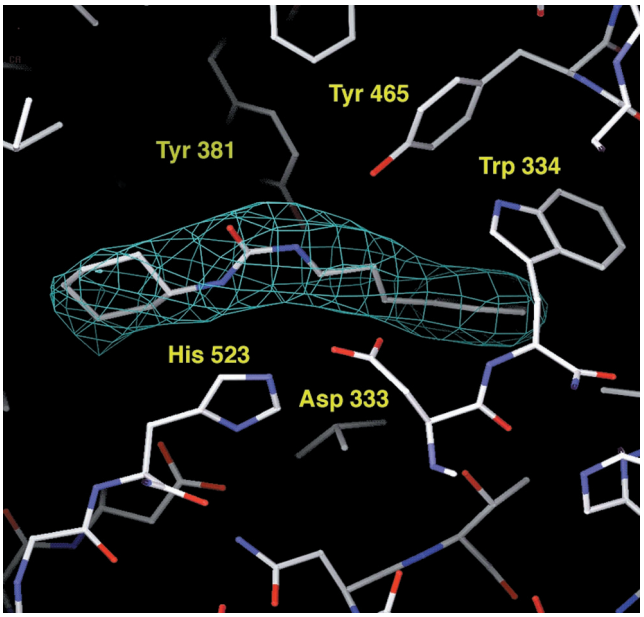

FIG. 2. Omit electron density map (contoured at 3.1σ) of the complex between sEH and the competitive inhibitor CPU (K_i = 3.1 nM). Note that the urea moiety of CPU binds with *cis*-(3-phenyl)propyl and *trans*-cyclohexyl amide linkages.

a severe health risk by compromising our ability to detoxify mutagenic and carcinogenic epoxides (32).

The three-dimensional structures of sEH and the sEH–CPU complex interpreted in light of available enzymological data allow us to summarize a detailed structure-based mechanism for the activation and hydrolysis of an epoxide substrate (Fig. 3). The carboxylate side chain of Asp-333 is the catalytic nucleophile (12–17); its orientation is fixed by polar interactions with His-523 and the backbone NH group of Phe-265. Directly across the active site cavity from Asp-333 is the phenolic side chain of Tyr-465, which is suitably oriented to serve as a possible general acid catalyst to activate and accelerate the opening of the epoxide ring; Tyr-465 is flanked by edge-to-face interactions with Trp-334 and Phe-385 that would stabilize the intermediate phenolate anion. Parenthetically, we note that the side chain of Tyr-381 is also nearby, but because it is further away from Asp-333 and because it is not conserved in mEH, Tyr-381 is a less likely possibility for the role of general acid catalyst. Substituent effects measured for substituted epoxide substrates suggest that epoxide ring opening proceeds by an S_N2-like mechanism rather than an S_N1-like mechanism involving formation of a substrate carbocation (42). This indicates that Tyr-465 and Asp-333 may function in concert to activate and open the epoxide substrate, resulting in the alkylenzyme ester intermediate. This is analogous to the role proposed for Tyr-215 and Asp-107 of the epoxide hydrolase from *Agrobacterium radiobacter* AD1 in an inactive conformation (38).

The alkylenzyme intermediate is subsequently hydrolyzed by a water molecule promoted by general base His-523, which must break its hydrogen bond with Asp-333 to allow for an intervening water molecule. The basicity of His-523 is enhanced by two residues: (*i*) the negatively charged carboxylate side chain of Asp-495, and (*ii*) the partial negative charge of the indole ring of Trp-524. The six-member ring portion of the indole ring contacts His-523; upon protonation of His-523, it can take part in a classic cation–π interaction (43) with Trp-524. It should be noted that all of the residues included in this mechanism are highly conserved in sEH and mEH as well as haloalkane dehalogenase. A notable exception is Tyr-465, which appears as phenylalanine in haloalkane dehalogenase. However, nucleophilic attack at the carbon–halogen bond in the first step of this enzyme mechanism does not require a proton donor because the negatively charged halide anion is a good leaving group. Thus, active site residues in each enzyme have diverged to accommodate strikingly different chemical steps required to hydrolyze xenobiotic substrates of highly variable chemical composition.

Vestigial Domain in Quaternary Structure Evolution. The N-terminal domain of sEH does not participate in epoxide hydrolysis, a conclusion based on ^{18}O incorporation experiments (12), site-directed mutagenesis of the catalytic domain (13, 31), and the binding of the inhibitor CPU exclusively in the catalytic domain (Fig. 1). Accordingly, we refer to the N-terminal domain as the vestigial domain. The vestigial domain bears some topology unexpectedly similar to haloacid dehalogenase despite inconclusively weak sequence identity of 20% (5, 29); however, sEH does not catalyze haloacid hydrolysis (unpublished results). Evolutionary remnants of a 13-Å-deep active-site cavity are clearly evident, with conservation of the key catalytic nucleophile (Asp-9 in sEH, and Asp-8 in haloacid dehalogenase (5, 18, 29)) and other active-site residues, with the exception of Arg-39 of haloacid dehalogenase (28, 29) (Fig. 4). Consequently, it is difficult to rationalize the lack of measurable catalytic function. The vestigial domain is unique to mammalian sEH and is not shared with mEH, plant epoxide hydrolases, or haloalkane dehalogenase (5). Possibly, the appropriate substrate for the active site of the vestigial domain has not yet been identified.

Alternatively, the vestigial domain may have diverged through evolution to serve a completely different biological function. Surprisingly, the crystal structure reveals that this domain plays a critical role in the stabilization of a distinctive quaternary structure: the catalytic and vestigial domains are intertwined with each other in a putative domain-swapped architecture (Fig. 1). "Domain-swapping" refers to an oligomeric structure in which one domain of a monomeric protein is displaced by the same domain of another monomer to form a stable dimer (44). Each sEH monomer adopts an open conformation in which the catalytic and vestigial domains are held apart from each other by the proline-rich linker. Neither

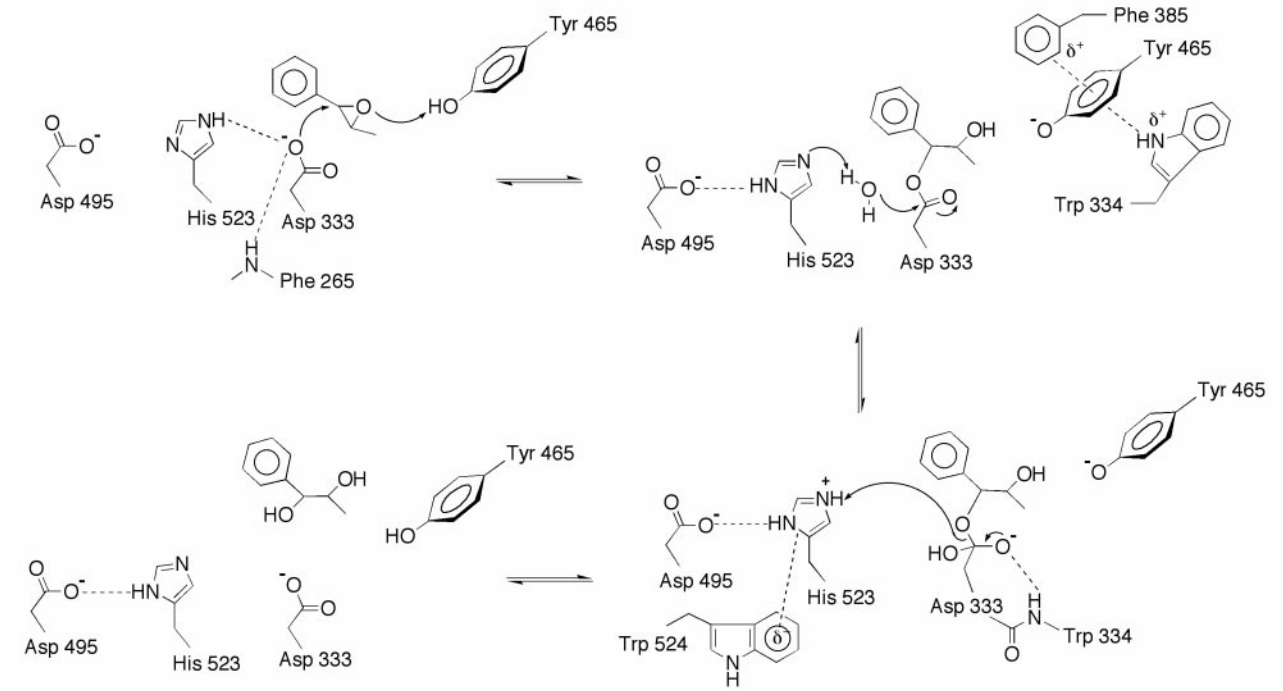

FIG. 3. Proposed mechanism of sEH in the hydrolysis of *trans*-β-methylstyrene oxide. Nucleophilic attack of Asp-333 yields the alkylenzyme ester intermediate, which is subsequently hydrolyzed (with the assistance of general base His-523) to yield the vicinal diol product.

the active site of the catalytic domain nor the active site of the vestigial domain is close to any interdomain or interprotein interface. Although there is no crystal structure yet of an sEH monomer, the observation of catalytic activity for sEH dimers *and* monomers (45, 46) in solution leads us to postulate the existence of a stable monomeric structure exhibiting the closed conformation illustrated in Fig. 5.

Given the genetic relationships between sEH and haloalkane and haloacid dehalogenases summarized in the previous section, and given the structural implications of domain swapping for the evolution of protein quaternary structure (44), a complete, structure-based evolutionary sequence can be postulated (Fig. 5). Briefly, an early gene fusion event linked the proteins ancestral to haloalkane and haloacid dehalogenase (5). Although the evolutionary driving force for the subsequent dimerization of the resultant two-domain protein is unknown, it is possible that dimerization conferred some unique advantage to the organism—e.g., metabolic regulation as the organism evolved to handle new and/or potentially toxic carbon sources. The linker segment between the two domains was sufficiently flexible to allow an equilibrium between closed and open conformations of the monomer, leading to the dimerization of two monomers in the open conformation. Subsequent destabilization of the closed conformation by amino acid substitutions in the hinge loop by incorporation of conformationally restrained proline residues (44) leads to increased stabilization of dimeric quaternary structure (the 16-residue linker between the vestigial and catalytic domains contains 5 proline residues). That an equilibrium between monomeric and dimeric sEH is implicated (45, 46) may indicate that the evolutionary change toward predominantly dimeric oligomerization remains in progress.

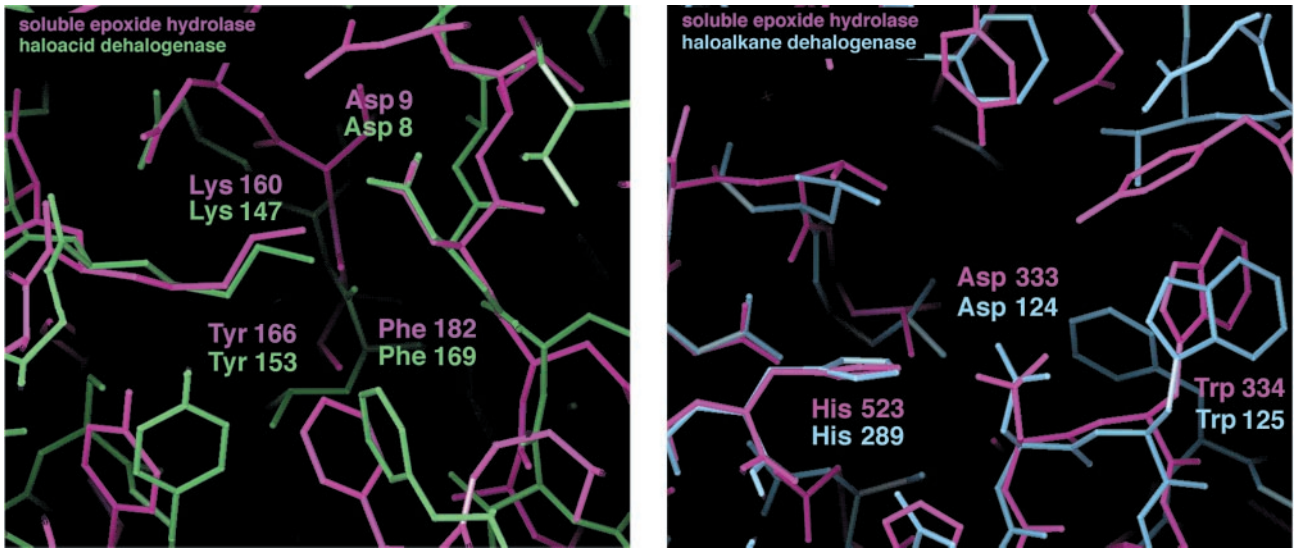

FIG. 4. (*Left*) Least-squares superposition of the vestigial active site of sEH with the active site of haloacid dehalogenase. (*Right*) Least-squares superposition of the active site of sEH with that of haloalkane dehalogenase.

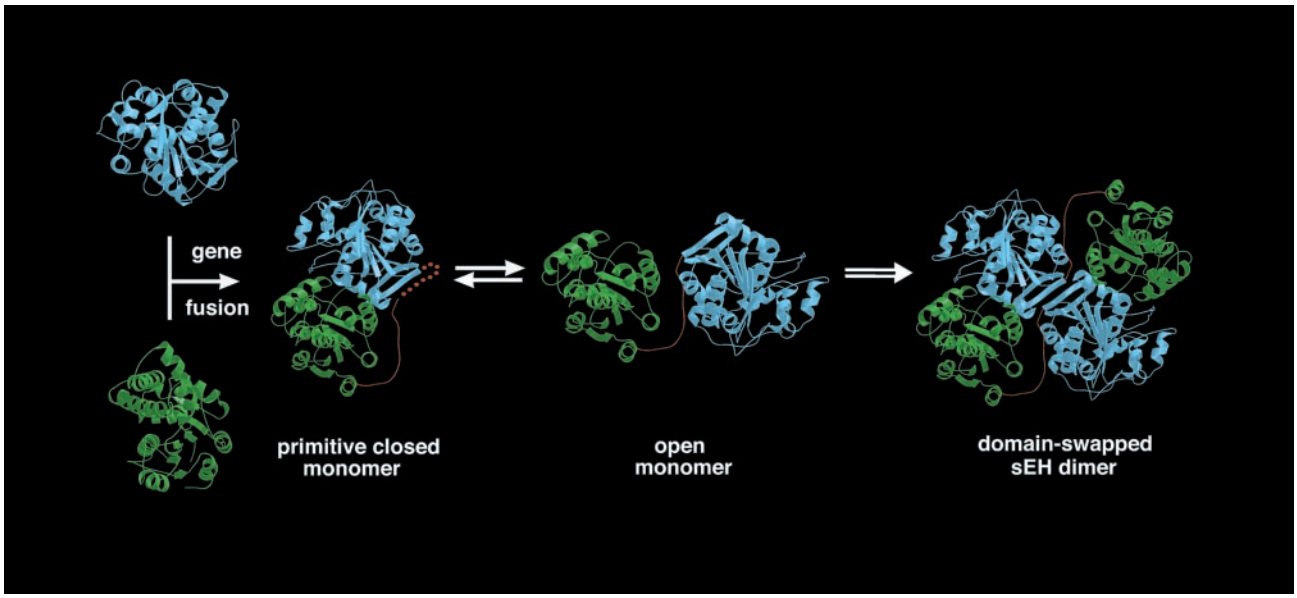

FIG. 5. Proposed structure-based evolutionary pathway of xenobiotic catabolism. Haloalkane dehalogenase (blue) and haloacid dehalogenase (green) ancestors underwent an early gene fusion event to yield a primitive monomeric protein adopting a postulated closed conformation. Subsequent equilibration with an open conformation and dimerization through domain-swapping is facilitated by a flexible linker (i.e., hinge loop; red); stabilization of the modern-day, domain-swapped sEH dimer is achieved through subsequent shortening and/or amino acid substitutions that rigidify the 16-residue linker, which in sEH contains 5 proline residues. This figure was prepared with BOBSCRIPT and RASTER3D (47–49).

The sEH inhibitor CPU was kindly provided by Dr. Marvin Goodrow. We thank Drs. D. Eisenberg, D. Elbaum, J. Feinman, C. A. Lesburg, R. Marmorstein, M. Titens, and T. Stams for helpful discussions. We are grateful to the Cornell High Energy Synchrotron Source (CHESS) and the National Synchrotron Light Source (NSLS) at the Brookhaven National Laboratory for beam time access. We thank the University of Pennsylvania Cancer Center Pilot Projects Program, the National Institutes of Health, and the National Institute of Environmental Health Sciences for support of this work. M.A.A. was supported in part by the University of Pennsylvania Plant Sciences Training Grant and the Nicholas Padis Graduate Fellowship from the Hellenic University Club of Philadelphia.

1. Wixtrom, R. N. & Hammock, B. D. (1985) in *Biochemical Pharmacology and Toxicology*, eds. Zakim, D. & Vessey, D. A. (Wiley, New York), Vol. 1, pp. 1–93.
2. Oesch, F. (1973) *Xenobiotica* **3,** 305–340.
3. Ota, K. & Hammock, B. D. (1980) *Science* **207,** 1479–1481.
4. Arand, M., Grant, D. F., Beetham, J. K., Friedberg, T., Oesch, F. & Hammock, B. D. (1994) *FEBS Lett.* **338,** 251–256.
5. Beetham, J. K., Grant, D., Arand, M., Garbarino, J., Kiyosue, T., Pinot, F., Oesch, F., Belknap, W. R., Shinozaki, K. & Hammock, B. D. (1995) *DNA Cell Biol.* **14,** 61–71.
6. Chang, C. & Gill, S. S. (1991) *Arch. Biochem. Biophys.* **285,** 276–284.
7. Eriksson, M., Zetterqvist, M. A., Lundgren, B., Andersson, K., Beije, B. & DePierre, J. W. (1991) *Eur. J. Biochem.* **198,** 471–476.
8. Arand, M., Knehr, M., Thomas, H., Zeller, H. D. & Oesch, F. (1991) *FEBS Lett.* **294,** 19–22.
9. Meijer, J. & DePierre, J. W. (1988) *Chem. Biol. Int.* **64,** 207–249.
10. El-Tantaway, M. A. & Hammock, B. D. (1980) *Mutat. Res.* **79,** 59–71.
11. Kramer, A., Frank, H., Setiabudi, F., Oesch, F. & Glatt, H. (1991) *Biochem. Pharmacol.* **42,** 2147–2152.
12. Borhan, B., Jones, A. D., Pinot, F., Grant, D. F., Kurth, M. J. & Hammock, B. D. (1995) *J. Biol. Chem.* **270,** 26923–26930.
13. Arand, M., Wagner, H. & Oesch, F. (1996) *J. Biol. Chem.* **271,** 4223–4229.
14. Hammock, B. D., Pinot, F., Beetham, J. K., Grant, D. F. & Oesch, F. (1994) *Biochem. Biophys. Res. Commun.* **198,** 850–856.
15. Lacourciere, G. M. & Armstrong, R. N. (1993) *J. Am. Chem. Soc.* **115,** 10466–10467.
16. Müller, F., Arand, M., Frank, H., Seidel, A., Hinz, W., Winkler, L., Hänel, K., Blée, E., Beetham, J. K., Hammock, B. D. & Oesch, F. (1997) *Eur. J. Biochem.* **245,** 490–496.
17. Laughlin, L. T., Tzeng, H.-F., Lin, S. & Armstrong, R. (1998) *Biochemistry* **37,** 2897–2904.
18. Pries, F., Kingma, J., Pentenga, M., van Pouderoyen, G., Jeronimus-Stratingh, C. M., Bruins, A. P. & Janssen, D. B. (1994) *Biochemistry* **33,** 1242–1247.
19. Franken, S. M., Rozeboom, H. J., Kalk, K. H. & Dijkstra, B. W. (1991) *EMBO J.* **10,** 1297–1302.
20. Verschueren, K. H. G., Franken, S. M., Rozeboom, H. J., Kalk, K. H. & Dijkstra, B. W. (1993) *J. Mol. Biol.* **232,** 856–872.
21. Verschueren, K. H. G., Seljée, F., Rozeboom, H. J., Kalk, K. H. & Dijkstra, B. W. (1993) *Nature (London)* **363,** 693–698.
22. Kurihara, T., Liu, J.-Q., Nardi-Dei, V., Koshikawa, H., Esaki, N. & Soda, K. (1995) *J. Biochem. (Tokyo)* **117,** 1317–1322.
23. Liu, J.-Q., Kurihara, T., Miyagi, M., Esaki, N. & Soda, K. (1995) *J. Biol. Chem.* **270,** 18309–18312.
24. Liu, J.-Q., Kurihara, T., Miyagi, M., Tsunasawa, S., Nishihara, M., Esaki, N. & Soda, K. (1997) *J. Biol. Chem.* **272,** 3363–3368.
25. U.S. Environmental Protection Agency (1992) *Federal Register* **57**, 31576 (July 16).
26. Ollis, D. L., Cheah, E., Cygler, M., Dijkstra, B., Frolow, F., Franken, S. M., Harel, M., Remington, S. J., Silman, I., Schrag, J., *et al*. (1992) *Protein Eng.* **5,** 197–211.
27. Hisano, T., Hata, Y., Fujii, T., Liu, J.-Q., Kurihara, T., Esaki, N. & Soda, K. (1996) *J. Biol. Chem.* **271,** 20322–20330.
28. Ridder, I. S., Rozeboom, H. J., Kalk, K. H., Janssen, D. B. & Dijkstra, B. W. (1997) *J. Biol. Chem.* **272,** 33015–33022.
29. Koonin, E. V. & Tatusov, R. L. (1994) *J. Mol. Biol.* **244,** 125–132.
30. Grant, D. F., Storms, D. H. & Hammock, B. D. (1993) *J. Biol. Chem.* **268,** 17628–17633.
31. Pinot, F., Grant, D. F., Beetham, J. K., Parker, A. G., Borhan, B., Landt, S., Jones, A. D. & Hammock, B. D. (1995) *J. Biol. Chem.* **270,** 7968–7974.
32. Morriseau, C., Goodrow, M., Dowdy, D., Zheng, J., Greene, J. F., Sanborn, J. R. & Hammock, B. D. (1999) *Proc. Natl. Acad. Sci. USA* **96,** 8849–8854.
33. Otwinowski, Z. & Minor, W. (1997) *Methods Enzymol.* **276,** 307–326.
34. Collaborative Computational Project, Number 4 (1994) *Acta Crystallogr. D* **50,** 760–763.
35. Abrahams, J. P. & Leslie, A. G. W. (1996) *Acta Crystallogr. D* **52,** 30–42.
36. Brünger, A. T., Kuriyan, J. & Karplus, M. (1987) *Science* **235,** 458–460.
37. Jones, T. A., Zou, J.-Y., Cowan, S. W. & Kjeldgaard, M. (1991) *Acta. Crystallogr. A* **47,** 110–119.

38. Nardini, M., Ridder, I. S., Rozeboom, H. J., Kalk, K. H., Rink, R., Janssen, D. B. & Dijkstra, B. W. (1999) *J. Biol. Chem.* **274,** 14579–14586.
39. Miyamoto, T., Silva, M. & Hammock, B. D. (1987) *Arch. Biochem. Biophys.* **254,** 203–213.
40. Dietze, E. C., Casas, J., Kuwano, E. & Hammock, B. D. (1993) *Comp. Biochem. Physiol.* **104B,** 309–314.
41. Dietze, E. C., Kuwano, E., Casas, J. & Hammock, B. D. (1991) *Biochem. Pharmacol.* **42,** 1163–1175.
42. Morisseau, C., Du, G., Newman, J. W. & Hammock, B. D. (1998) *Arch. Biochem. Biophys.* **356,** 214–228.
43. Ma, J. C. & Dougherty, D. A. (1997) *Chem. Rev.* **97,** 1303–1324.
44. Bennett, M. J., Schlunegger, M. P. & Eisenberg, D. (1995) *Protein Sci.* **4,** 2455–2468.
45. Gill, S. S. (1983) *Biochem. Biophys. Res. Commun.* **112,** 763–769.
46. Dietze, E. C., Magdalou, J. & Hammock, B. D. (1990) *Int. J. Biochem.* **22,** 461–470.
47. Esnouf, R. M. (1997) *J. Mol. Graphics* **15,** 132–134.
48. Bacon, D. J. & Anderson, W. F. (1988) *J. Mol. Graph.* **6,** 219–220.
49. Merritt, E. A. & Murphy, M. E. P. (1994) *Acta Crystallogr. D* **50,** 869–873.